Smart Mater. Struct. **20** (2011) 115012 (5pp) doi:10.1088/0964-1726/20/11/115012

# Composites with mechanically tunable plasmon frequency

**Crystal J Schuil[1], Alireza V Amirkhizi, Farhad Bayatpur and Sia Nemat-Nasser**

Center of Excellence for Advanced Materials, Department of Mechanical and Aerospace Engineering, University of California, San Diego, CA, USA

E-mail: sia@ucsd.edu

Received 15 March 2011, in final form 28 July 2011
Published 11 October 2011
Online at stacks.iop.org/SMS/20/115012

**Abstract**

This paper summarizes our efforts to create a composite material with a mechanically tunable plasmon frequency at the microwave band. The permittivity of the composite changes sign at the plasmon frequency. Such composites, therefore, can be used as electromagnetic filters. Theoretically, an array of non-magnetic, metallic wire coils has been shown to have a plasmon behavior that is dependent on the wire thickness, coil inner diameter, pitch and coil spacing. Here, a material is made out of an array of coils placed within a non-metallic frame, and the material plasmon frequency is tuned through altering the pitch. The coils are arranged with alternating handedness to create an effective, non-chiral medium. A transmit/receive setup is used to characterize the electromagnetic behavior of the composite. The setup consists of a vector network analyzer and two horn antennas, which are used to measure the scattering parameters of the material. These parameters are then used to calculate the permittivity. The results show an increase in the plasmon frequency with increase in the pitch. Increasing the pitch 30%, from 3 to 3.9 mm, results in a corresponding increase from 6.3 to 7.5 GHz in the frequency.

(Some figures in this article are in colour only in the electronic version)

## 1. Introduction

The electromagnetic wave propagation in a non-chiral material is determined by two constitutive parameters [1]: permittivity ($\epsilon$) and permeability ($\mu$). In a plasmonic material, $\epsilon$ switches from a negative value to a positive one, as the frequency increases. This results in the index of refraction, the wavenumber, and the wave impedance changing from imaginary values to real values. Before this transitional frequency, the electromagnetic waves decay exponentially in the material according to Maxwell's equations, and therefore the material is reflective. With the permittivity being positive above the plasmon frequency, the electromagnetic waves are transmitted harmonically through the material, thus implying the wave propagation inside the material. Given its transitional effect, the plasmon frequency is also frequently referred to as the turn-on frequency [2]. Exhibiting highly dispersive electromagnetic behavior, such structures have applications in design of reconfigurable communication systems, including polarizers and impedance layers [3, 4]. This paper explores the mechanical tuning of the metal–dielectric composites with a plasmonic behavior in the microwave regime [2, 5].

An array of thin, straight wires supported by a dielectric material was shown to have a plasmonic behavior [6, 7]. To achieve this at microwave frequencies, the ratio of the wire spacing to the wire diameter must be very large (∼100) [8]. This makes the fabrication of such arrays cumbersome. However, since the effective permittivity of the wire array is also affected by the self-inductance of the array elements, the introduction of helical wires (wire loops [8]) makes it possible to use thicker wires and smaller unit cells. This can help to ease the process of manufacturing such composites. Using conductive coils also introduces more design parameters. Coils may be either left- or right-handed. Embedding same-handed coils in a composite introduces chirality in to the system [3]. The analysis and modeling of such chiral composites have been the subject of extensive research in recent years [9–11].

[1] Current address: Schlumberger Ltd., Houston, TX, USA.

 

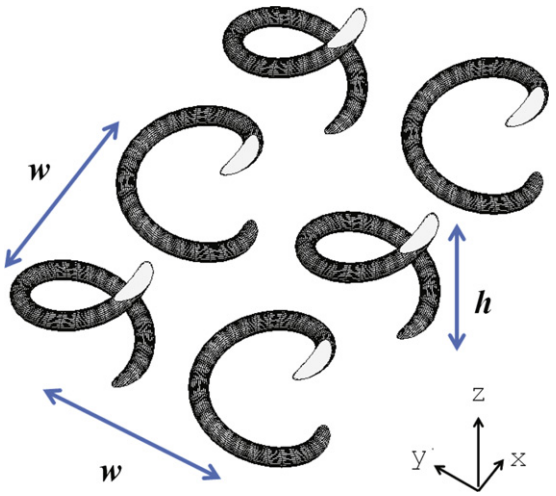


**Figure 1.** Unit cell geometry of the spring array. The array is three layers thick ($\hat{x}$) and is periodic along $\hat{y}$ and $\hat{z}$. The springs in this picture alternate between left-handed and right-handed.

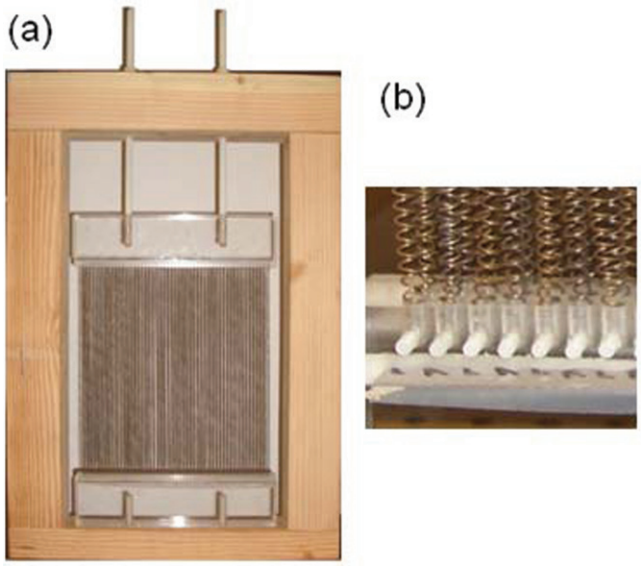


**Figure 2.** (a) Test frame and (b) screws holding springs in place on the base.

One method for suppressing the chirality is to use a setup that alternates between left-handed and right-handed coils. Another way uses double coils. A double coil has two wires that are wound in opposite directions [2, 5].

A periodic array of conducting elements can be treated as an effective medium for electromagnetic scattering so long as the wavelength of operation is much larger (>10) than the array periodicity [12]. Arrays of coils have been numerically studied to determine the variations of the plasmon frequency for selections of pitch, inner diameter, wire radius, and unit cell width [5]. Here, we demonstrate a helix composite whose plasmonic properties can be tuned through mechanical tuning of the helix pitch. Essentially, tuning the pitch tunes the level of self-inductance of the helix; the smaller the pitch, the higher the self-inductance. A higher self-inductance in turn decreases the plasmon frequency [6, 8].

## 2. Design and fabrication

The unit cell geometry (one period) of the spring array is shown in figure 1. This array has three layers of springs that are periodic along $\hat{y}$ and $\hat{z}$. A low-frequency band of operation is chosen here to allow for relatively large dimensions for the springs, thus avoiding fabrication difficulties. In order to achieve a plasmon frequency in the desired range (6–9 GHz), it is necessary to scale the numerical calculations given in [5]. Without scaling, the plasmon frequencies are higher than the desired range. Pendry *et al* [6], developed the relationship between self-inductance of scatterers, their spacing and the plasmon frequency. Here, we have optimized the design values such that the operation band will be around 6–9 GHz, where we perform the measurement. The spring array dimensions are provided in table 1. In this table, $h$ is the periodicity along $\hat{z}$, $w$ is the spacing of the coils in $\hat{x}$ and $\hat{y}$ directions, $d$ is the spring inner diameter, $t$ is the wire thickness, and $L_0$ is the spring length at rest. In this array, each pair of neighboring coils have opposite directions, which in turn suppresses the chirality. For the coils' fabrication, beryllium copper, which is a non-magnetic material, was selected. The coils were then placed in an array fashion and held parallel with one another using a test frame. The frame was made out of wood, to avoid (reflection) electromagnetic interference with coils, and designed such that it can support the maximum expected force. Given the number of the coils, their maximum extension, and the type of material used for their fabrication, the maximum force was estimated to be 15.3 N at 40% coils' extension, using the following expression:

**Table 1.** Spring array design parameters' values (mm).

| $h$ | $w$ | $d$ | $t$ | $L_0$ |
|---|---|---|---|---|
| 2.9 | 6 | 3 | 0.57 | 318 |

$$K_{\text{spring}} = \frac{Gt^4}{8nD^3}$$

where $G$ is the shear modulus; $t$ is the wire thickness; $D$ is the diameter, and $n$ is the number of coils. The prototype sample shown in figure 2 was fabricated including an array of 3 × 56-element, alternating springs in a wooden frame.

## 3. Analysis and measurement

### *3.1. Permittivity and permeability retrieval*

The permittivity of the coil array is extracted in this section [13, 14]. Above the plasmon frequency of a non-magnetic material the permittivity is positive and real, and the permeability is approximately equal to that of free space (≈1). Given these assumptions, the permittivity is extracted from the changes in the phase of a wave passing through the material. This method needs an accurate measurement of the material thickness.

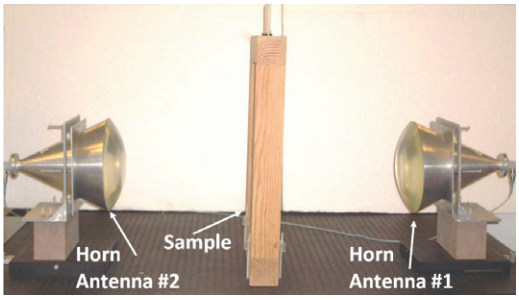


**Figure 3.** Measurement setup for testing the spring material. The horn antennas are connected to a VNA.

Below the plasmon frequency, however, the array becomes highly reflective because of an imaginary wavenumber. In this case, both transmission and reflection properties of the material under test are needed in the retrieval process. Here, a method presented earlier in [13, 15] is used. This method requires accurate measurement of the material's reflection ($S_{11}$) and transmission ($S_{21}$) coefficients. These $S$-parameters are measured at either interfaces of the material with air. The calculation starts with defining two parameters, $\Gamma$ and $T$, as follows:

$$T = \mathrm{e}^{-\gamma d} \tag{1}$$

$$\Gamma = \frac{Z-1}{Z+1} \tag{2}$$

where $\gamma = \gamma_\mathrm{o}\sqrt{\mu\epsilon}$ and $Z = \sqrt{\mu/\epsilon}$ are the propagation constant and the wave impedance inside the material, respectively. $\gamma_\mathrm{o} = 2\pi f\sqrt{\mu_\mathrm{o}\epsilon_\mathrm{o}}$ is the free space propagation constant.

Given the measured $S_{11}$ and $S_{21}$, it can be shown that for a slab material in a free space environment, the following relations hold [13]:

$$S_{11} = \frac{\Gamma(1-T^2)}{1-T^2\Gamma^2} \tag{3}$$

$$S_{21} = \frac{T(1-\Gamma^2)}{1-T^2\Gamma^2}. \tag{4}$$

Calculating $\Gamma$ and $T$ from equations (3)–(4), we obtain [15],

$$\Gamma = K \pm \sqrt{K^2-1} \tag{5}$$

$$T = \frac{S_{11}+S_{21}-\Gamma}{1-(S_{11}+S_{21})\Gamma} \tag{6}$$

where

$$K = \frac{{S_{11}}^2 - {S_{21}}^2 + 1}{2S_{11}}.$$

Equations (5)–(6) allow for extraction of $\Gamma$ and $T$ from the measured results. These parameters are then used in equations (1)–(2) to retrieve the propagation constant and the impedance, which are directly related to $\epsilon$ and $\mu$.

### *3.2. Electromagnetic experiment*

As mentioned earlier, $S$-parameters are needed for the characterization of the coil array. A conventional transmit/receive (TR) setup is used to obtain the scattering response. The measurement setup consists of two lens-horn antennas and an 8510C vector network analyzer (VNA) [15]. This setup is shown in figure 3. The horn antennas have a focal length of ∼35 cm. This means the horns should be placed 70 cm apart with the slab material in between. The antennas operate in the band 6.2–8.4 GHz. Prior to measurement, the setup is calibrated using the TRL (Thru-Reflect-Line) method [16–18]. Time domain gating can also be used in conjunction with the calibration to minimize the effects of residual timing mismatch [19]. Using this setup, scattering ($S_{11}$ and $S_{21}$) parameters of the spring array are measured.

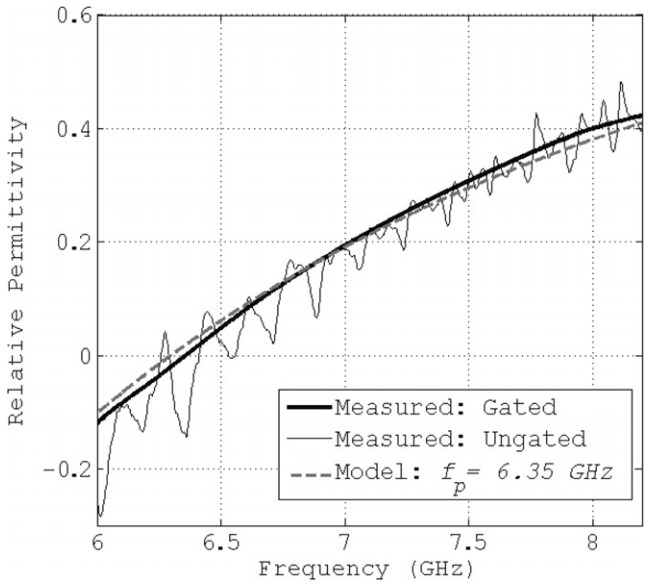


**Figure 4.** Calculated springs' relative permittivity (real part) using calibrated and ungated/gated measured data compared with the Drude–Lorentz model. Solid lines are calculated from the data, and the dashed line is from the model. Gating helps to smooth the measured results by eliminating undesired reflections from the sample under test.

### *3.3. Analysis and measurement results*

In this section, the spring array is characterized using the method described above. The electromagnetic test (see section 3.2) is first performed to measure the scattering response of the array from 6 to 8.4 GHz. The setup is calibrated, and time domain gating is used to further polish the data. Given the measured data, the permittivity is next extracted using the analysis presented in section 3. The measured permittivity compared with the best fit of Drude–Lorentz model for plasmonic materials is provided in figure 4, showing a good agreement between the model and the measurement. This model establishes a relation between the relative permittivity ($\epsilon_\mathrm{r}$) and the plasmon frequency ($f_\mathrm{p}$) at each frequency ($f$) [20].

$$\epsilon_\mathrm{r} = 1 - \frac{{f_\mathrm{p}}^2}{f^2}. \tag{7}$$

Figure 4 also demonstrates the effect of the time domain gating on the measured results. Gating is a feature in VNA that can

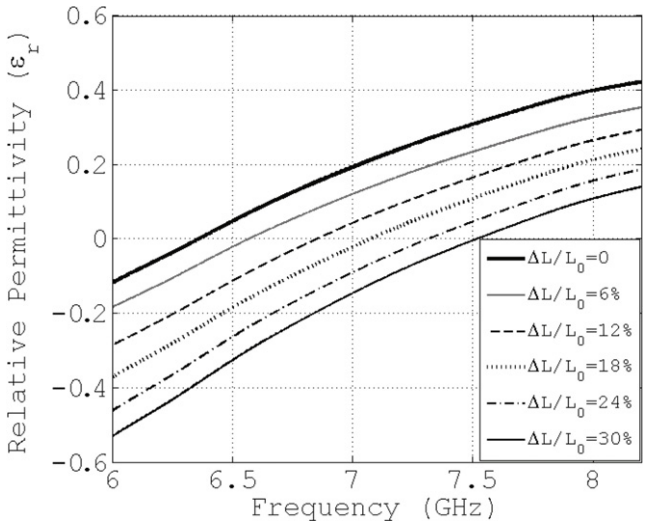


**Figure 5.** Calculated springs' relative permittivity (real part) at different extensions ($\Delta L$), from 0 to 30%, using calibrated and gated measured data. Imaginary part of the permittivity remains almost constant and close to zero in the entire band.

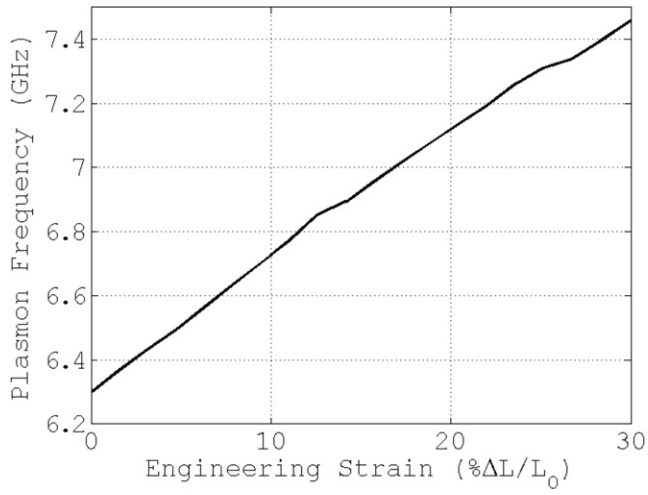


**Figure 6.** Mechanical tuning of the plasmon frequency for a $3 \times 56$-element array of springs. ∼17% frequency tuning is achieved by 30% extension in the springs' length.

be utilized to selectively remove transmission and reflection responses. In this measurement, turning the gate function on helps to further remove undesired reflections from the material under test, thus achieving a smoother response.

The permittivity is calculated next, using the calibrated and gated data measured at different levels of extension of the array. The array length is increased 6% at each step up to 30%. As shown in figure 5, by increasing the spring pitch ($h$), the plasmon frequency is increased. Figure 6 shows the variations of the plasmon frequency as a function of the extension length. An increase of the frequency by ∼1.2 GHz is established from the measurements.

To test the effect of the thickness on the permittivity, the spring array is reduced to only two layers for another set of measurements. In order to accurately monitor the

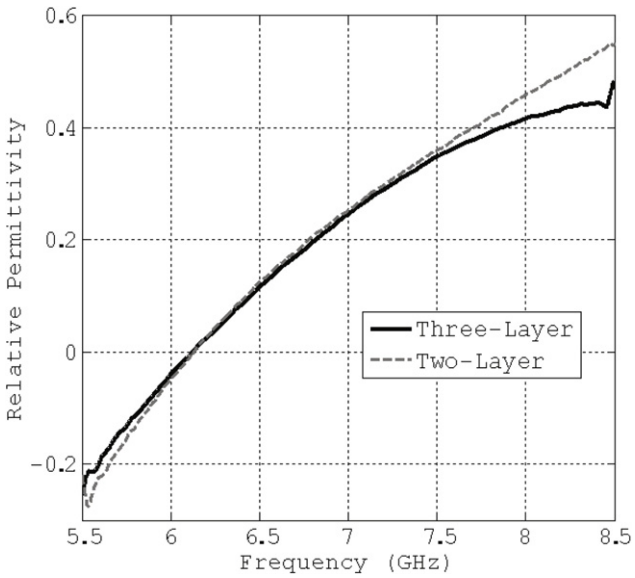


**Figure 7.** Calculated springs' relative permittivity (real part) using calibrated and gated measured data for the thinner array ($2 \times 56$-element) compared with that of the three-layer array.

thickness effect, the band of measurement is slightly increased from the nominal band (6.2–8.4 GHz) to 5.5–8.5 GHz. The antennas are fully calibrated again in the new band. The calculated permittivity for the thinner array is shown in figure 7, exhibiting a behavior similar to that of the three-layer array. As expected, at lower frequencies the array can be approximated as an effective medium with a single overall permittivity value. However, the permittivity difference between the two- and three-layer arrays at higher frequencies invalidates the existence of an effective dielectric property. This is due to the increased length of the periodicity compared to the wavelength.

The new measurement (figure 7) compared to the initial measurement (figure 4), predicts a slightly lower plasmon frequency. Although minor, this deviation is partly due to the calibration. For TRL calibration of the measurement setup, three physical standards are used. Each standard is placed between the two antennas so that the VNA measures the necessary $S$-parameters for calculating the calibration coefficients. More error could affect this calculation if the standards are misplaced within a fraction of the wavelength. At the frequency band of operation, each millimeter variation in distance changes the phase of the measured $S$-parameters by ∼10° on average. In addition to the calibration accuracy, the second measurement (figure 7) was done after one full stretch of the coils up to 30% which could change the coils' arrangement in the array.

## 4. Conclusions

The plasmon frequency of a composite with coiled wire arrays is dependent on four parameters: unit cell width, wire thickness, coil inner diameter, and pitch. Here, three of those parameters were held constant. The pitch was mechanically adjusted. Previous theoretical studies on increasing the pitch

of the coil showed that the plasmon frequency should also increase. This paper experimentally demonstrated that it is possible to create composites with mechanically adjustable plasmon frequencies. An array of springs with alternating handedness was fabricated. Through the use of a TR setup, free space material measurements were performed on the spring array. Mechanical tuning of the plasmon frequency was achieved by 30% extending the springs. An increase of the frequency by ∼1.2 GHz was observed experimentally.

## Acknowledgments

This work has been supported in part by AFOSR/MURI grant FA9550-06-1-0337 to Kent State University, sub-award 44286-P061719 to the University of California, San Diego, and in part by AFOSR grant FA9550-09-1-0528 to the University of California, San Diego. The authors would like to thank Mr Jon Isaacs for his assistance in this work.

## References

[1] Kong J A 2000 *Electromagnetic Wave Theory* (Cambridge, MA: EMW Publishing) chapter 2

[2] Nemat-Nasser S, Nemat-Nasser S, Plaisted T, Starr A and Amirkhizi A V 2005 *Multifunctional Materials, Biomimetics: Biologically Inspired Technologies* ed B-C Yoseph (Boca Raton, FL: CRC Press) chapter 12

[3] Lindell I V and Sihvola A H 1995 Plane-wave reflection from uniaxial chiral interface and its application to polarization transformation *IEEE Trans. Antennas Propag.* **43** 1397–404

[4] Alekseyev L V, Narimanov E E, Tumkur T, Li H, Barnakov Yu A and Noginov M A 2010 Uniaxial epsilon-near-zero metamaterial for angular filtering and polarization control *Appl. Phys. Lett.* **97** 131107

[5] Amirkhizi A V 2006 Multifunctional composites and structures with integrated mechanical and electromagnetic properties *Doctorate Thesis* University of California, San Diego

[6] Pendry J B, Holden A J, Stewart W J and Youngs I 1996 Extremely low frequency plasmons in metallic mesostructures *Phys. Rev. Lett.* **76** 4773–6

[7] Gay-Balmaz P, Maccio C and Martina O J F 2002 Microwire arrays with plasmonic response at microwave frequencies *Appl. Phys. Lett.* **81** 2896–8

[8] Smith D R, Vier D C, Padilla W, Nemat-Nasser S C and Schultz S 1999 Loop-wire medium for investigating plasmons at microwave frequencies *Appl. Phys. Lett.* **75** 1425–7

[9] Silveirinha M G 2008 Design of linear-to-circular polarization transformers made of long densely packed metallic helices *IEEE Trans. Antennas Propag.* **56** 390–401

[10] Amirkhizi A V and Nemat-Nasser S 2008 Numerical calculation of electromagnetic properties including chirality parameters for uniaxial bianisotropic media *Smart Mater. Struct.* **17** 015042

[11] Gansel J K, Thiel M, Rill M S, Decker M, Bade K, Saile V, von Freymann G, Linden S and Wegener M 2009 Gold helix photonic metamaterial as broadband circular polarizer *Science* **325** 1513–5

[12] Weiglhofer W S, Lakhtakia A and Monzon J C 1993 Maxwell–Garnett model for composites of electrically small uniaxial objects *Microw. Opt. Technol. Lett.* **6** 681–4

[13] Nicolson A M and Ross G F 1970 Measurement of the intrinsic properties of materials by time domain techniques *IEEE Trans. Instrum. Meas.* **19** 377–82

[14] Chen L F, Ong C K, Neo C P, Varadan V V and Varadan V K 2004 *Microwave Electronics: Measurement and Materials Characterization* (Chichester: Wiley) pp 142–205

[15] Ghodgaonkar D K and Varadan V V 1990 Free space measurement of complex permittivity and complex permeability of magnetic materials at microwave frequencies *IEEE Trans. Instrum. Meas.* **39** 387–94

[16] Engen G F and Hoer C A 1979 Thru-reflect-line: an improved technique fo calibrating the dual six-port automatic network analyzer *IEEE Trans. Microw. Theory Technol.* **27** 987–93

[17] Agilent 2006 *Agilent Network Analysis Applying the 8510 TRL Calibration for Non-Coaxial Measurements* (Santa Clara, CA: Agilent Technologies) 5091–3645E

[18] Agilent 2006 *Agilent Specifying Calibration Standards for the Agilent 8510 Network Analyzer* (Santa Clara, CA: Agilent Technologies) 5956-4352

[19] Agilent 2007 *Agilent Time Domain Analysis Using a Network Analyzer* (Santa Clara, CA: Agilent Technologies) 5989–5723EN

[20] Bohren C and Huffman D 1983 *Absorption and Scattering of Light by Small Particles* (New York: Wiley)